International Journal of Heat and Mass Transfer 196 (2022) 123256

Contents lists available at ScienceDirect

International Journal of Heat and Mass Transfer

journal homepage: www.elsevier.com/locate/hmt

Hydraulic characterization and modeling of water diffusivity through direct neutron radiography measurement on unsaturated cracked sandstone

Yixin Zhao[a,b,c,*], Yang Wu[a,c], Chuanlong Dong[a,c], Songbai Han[d], Derek Elsworth[f], Linfeng He[e]

[a] Beijing Key Laboratory for Precise Mining of Intergrown Energy and Resources, China University of Mining and Technology (Beijing), Beijing 100083, China
[b] State Key Laboratory of Coal Resources and Safe Mining, China University of Mining and Technology, Beijing 100083, China
[c] School of Energy & Mining Engineering, China University of Mining and Technology, Beijing 100083, China
[d] Academy for Advanced Interdisciplinary Studies, Southern University of Science and Technology, Shenzhen 518055, China
[e] Neutron Scattering Laboratory, China Institute of Atomic Energy, Beijing 102413, China
[f] Department of Energy and Mineral Engineering, G3 Center and Energy Institute, The Pennsylvania State University, University Park, PA 16802, USA

ARTICLE INFO

Article history:
Received 8 September 2021
Revised 8 February 2022
Accepted 14 July 2022

Keywords:
Hydraulic diffusivity
Neutron radiography
Time exponent
Diffusivity model
Models comparison

ABSTRACT

Water diffusivity in cracked rocks is of great importance in the recovery of conventional and unconventional resources and in the sequestration of carbon dioxide and nuclear wastes. However, the mechanism of water diffusivity is not clearly revealed in the unsaturated fractured sandstone due to the limitation of accurately identifying the dynamic wetting front and water content in the conventional methods. Based on a set of self-designed coupling loading device, the novel neutron radiography imaging is used to visualize the dynamic diffusivity process of forced water from a horizontal rough crack vertically imbibed into an unsaturated sandstone matrix with nonuniform boundary in real time. As a result, an anomalous diffusivity phenomenon, namely the time exponent less than 0.5 is discovered. The anomalous diffusivity may be mainly caused by the heterogeneity and anisotropy of matrix and complicated 3-D water imbibition due to nonuniform geometric boundary. The nonstandard imbibition experiment condition may be an additional important factor. The anomalous diffusivity was calculated by three methods, including the Generalized Fickian law, Lockington and Parlange (L-P) model and the developed Meyer-Warwick (M-W) model. The value of the diffusivity increases non-linearly with the increase of normalized water content θ_n. The diffusivity calculated by the developed M-W model increases rapidly with increasing θ_n from 0 to 0.2 mm^3mm^{-3}, which is almost the same as that calculated by L-P model. When $\theta_n > 0.2$ mm^3mm^{-3}, the L-P model obviously overestimates the diffusivity, but the diffusivity calculated by the developed M-W model is closest to that obtained by the Generalized Fickian law. The developed M-W model provides an effective way to quantitatively describe the diffusivity of water in the sandstone matrix.

1. Introduction

Natural and artificial porous materials containing fractures and/or cracks are ubiquitous, and most of them are partially saturated with various fluids. Water associated with the dissolved minerals and particulates can imbibe and penetrate into the porous materials quickly through the open cracks. The fundamental understanding and modeling of the hydro-dynamical process is of great importance for practical application in many fields, including the exploitation of energy reservoirs [1–3] (such as oil, natural gas), the underground sequestration or storage of gaseous or solid waste [4–7] (such as carbon dioxide, nuclear waste), and the protection of building or structure materials [8] (such as sandstone, concrete, reinforced concrete). The water diffusivity within cracked porous media is well known to be a complex dynamic physical process, particularly for the observed anomalous water diffusivity phenomena in recent years. The fundamental understanding of water diffusivity plays an important role in accurately describing water transport through the unsaturated fractured porous media.

Commonly, the sorptivity and diffusivity coefficients are used to define transient water transport in porous materials under partially-saturated conditions [9], and these two quantities are implicitly appeared as the dynamic evolution of the wetting front in

* Corresponding author at: Beijing Key Laboratory for Precise Mining of Intergrown Energy and Resources, China University of Mining and Technology (Beijing), Beijing 100083, China.
E-mail address: zhaoyx@cumtb.edu.cn (Y. Zhao).

https://doi.org/10.1016/j.ijheatmasstransfer.2022.123256
0017-9310/

macroscopic-scale. Two traditional methods including the weighting [10,11] and instantaneous profile [9] are frequently used to determine unsaturated diffusivity. However, the reliability and accuracy of these two traditional methods in the prediction of the dynamic water distribution during water diffusivity process has been questioned [9]. With the development of non-destructive experimental imaging techniques, such as Nuclear Magnetic Resonance [12,13], X-ray imaging [14,15] and neutron imaging [16–19], the ability to visualize fluid flow in time series for unsaturated porous, fractured materials has increased in most recent years. Although Nuclear Magnetic Resonance [12,13] and X-ray imaging [20,21] are still used to research unsaturated water flow and diffusivity in porous materials, both of them have their own limitations. For instance, X-ray imaging can clearly observe the migration and distribution of water only through the use of contrast agents [22] (e.g., cesium chloride and salts), which may alter the wetting behavior of the porous media (e.g., the contact angle of water to solid) [9,23]. Nuclear Magnetic Resonance cannot measure the accurate spatial water content due to its limit of the pore size range [24] and the presence of mineral element (e.g., iron) in porous media [25]. In contrast, the neutron radiography technology is one of the best methods to investigate the water transport dynamics in porous materials [19,26]. Because neutrons are strongly attenuate by hydrogen and relative insensitivity to gas and solid components (e.g., quartz) [18]. Thus, the neutron radiography has been widely applied to capture the variety of water content during water imbibition in both natural and engineering porous materials, such as brick, concrete, porous glass, sand, rock and soil [18,27–32].

The natural rocks, even for tight sandstone and shale have strong heterogeneity and anisotropy which have considerable effect on the mechanical [33] and hydraulic [34] property in the microscopic perspective due to the certain flaw of natural generation. The anisotropy leads to the directionality of hydraulic characterization including saturated permeability and unsaturated imbibition, namely there is prominent difference for penetration characteristics in different directions [35]. The heterogeneity contributes to the temporal variation of hydraulic characteristics, that is, there is different penetration characteristics in different position [36]. Hence, the two characteristics (i.e., heterogeneity and anisotropy) can comprehensively gave rise to complicated unsaturated penetration including the nonstandard hydraulic diffusivity property [37] and nonuniform wetting evolution law [38] in comparison to the isotropical homogeneous artificial materials.

The studies of the water imbibition hydraulics in unsaturated porous media can be traced back to the beginning of the 20th century when the basic understanding of the capillary laws universally finding that the linear relationship between the wetting front position L and the square root of time was gained as the later recognized L-W equation [39–45]. The L-W equation lays the foundation for the study of water imbibition in porous materials. Based on L-W equation and combined with Richard's equation, Fick's law and Boltzmann transform, many studies proved an experimental phenomenon described by L-W laws in the unsaturated diffusivity and imbibition of water in both matrix and crack of the porous materials by using neutron radiography technology [8,9,26,46–51]. However, A series of increasing experimental and theoretical analyses on the liquid wetting behavior of porous media suggested that the dynamic evolution of the water wetting front did not always follow the classical L-W equation (i.e., the time exponent is not 0.5) [52], which may be caused by these mechanisms such as the complex micro-structure [53–55], fractal characteristics [56,57], non-Newtonian behavior [58,59], and the chemo-mechanical changes [58]. Thus, the accuracy of hydraulic diffusivity of the porous materials predicted by L-W equation has been increasingly questioned. In other words, previous researches imply that the evolution of the wetting front significantly deviates from the Boltzmann scaling, reflecting the anomalous Boltzmann scaling (i.e., non-Boltzmann scaling) [60]. The ordinary differential unsaturated diffusivity equation derived based on the non-Boltzmann transform deviates from the classical diffusivity equation. A few unique terminologies, such as '*anomalous diffusivity*' [16,61,62], '*hyper/hypo-diffusivity*' [63] or '*super/sub-diffusivity*' [64], were used to emphasize and distinguish this phenomenon. With the observed anomalous diffusivity phenomenon of porous media, a few developed theoretical models are proposed to describe the anomalous phenomenon by using the generalized Fick's law [16,62], fractal ruler [60,65] and fractional order [66,67].

However, the previous studies mostly focused on the diffusivity of water in unsaturated porous media matrix with uniform boundary conditions where the liquid surface remained static and in the absence of forced pressure [68]. The diffusivity of water in fractured unsaturated porous media with nonuniform geometry has not been fully characterized, especially the influence of microstructure on the diffusivity behavior. Therefore, in this study the water transport behavior and dynamic evolution from the horizontal roughness fracture to the matrix were continuously monitored by utilizing the neutron radiography imaging under the forced pressure. According to the corrected neutron radiography experimental data, the anomalous diffusivity phenomenon of water was found as a result of time exponent less 0.5 in the rock matrix along with its mechanism analysis. Moreover, three existing models, including the Generalized Fickian law [16,62], L-P model [58] and the modified Meyer-Warwick model (W-M model) [16], were employed to calculate the diffusivity of the cracked sandstone specimen, comparatively.

2. Theoretical framework

To quantitatively define anomalous water diffusivity behaviors in unsaturated porous media, theories and the corresponding analytical methods have been proposed and established [16,60,66]. By combining the unsaturated hydraulic conductivity function and the capillary pressure-saturation function [50] or employing horizontal infiltration method [69], the unsaturated diffusivity can be directly obtained. Recently, some fractal theory-based models have been proposed to predict the unsaturated diffusivity [70,71]. Generalization of the diffusivity equation, derived through the generalized Fickian law with the non-Boltzmann transformation, was introduced to describe the diffusivity. Theoretical models of Lockington, Parlange and Meyer-Warwick define the anomalous diffusivity functions. The use of a fractal derivative has been found to be effective in simulating anomalous diffusivity processes [72,73] and can be applied [74] to model a variety of power law scaling phenomena.

2.1. Diffusivity based on generalized Fickian law

Diffusivity is an effective physical parameter, which was used to investigate the dynamic imbibition process in unsaturated porous media [16,18,75]. In order to eliminate the influence of time on diffusivity, the Fickian exponent has been introduced. The gravity was assumed negligible and the process of the flow was then reduced to one-dimensional transport. The Generalized Fick's law can be expressed as [16]

$$Q = -D(\theta_n)\frac{\nabla\theta_n}{|\nabla\theta_n|}|\nabla\theta_n|^{\gamma} \tag{1}$$

where Q is the flux of water, $D(\theta_n)$ is diffusivity function, θ_n [mm^3mm^{-3}] is the normalized volumetric water content, $\theta_n = (\theta-\theta_i)/(\theta_s-\theta_i)$, θ [mm^3mm^{-3}] is the volumetric water content, θ_i[mm^3mm^{-3}] is the initial volumetric water content, θ_i=0, θ_s[mm^3mm^{-3}] is the saturated volumetric water content, θ_s=0.09,

$\nabla\theta_n$ is the normalized volumetric water content gradient, γ is the Fickian exponent. Applying the continuity equation, the Eq. (1) can be transformed to a generalized diffusivity equation for water content as:

$$\frac{\partial\theta_n}{\partial t} = \nabla\left(D(\theta_n)\frac{\nabla\theta_n}{|\nabla\theta_n|}|\nabla\theta_n|^{\gamma}\right) \tag{2}$$

Considering the boundary conditions, $\theta_n(L,0)=\theta_i$ and $\theta_n(0,t)=1$, and applying the non-Boltzmann variable $\varphi = Lt^{-\alpha}$ (α is the time exponent), the Eq. (2) can be reduced to an ordinary differential equation as:

$$\alpha\varphi\frac{d\theta_n}{d\varphi} = -t^{1-\alpha(1+\gamma)}\frac{d}{d\varphi}\left(D(\theta_n)\mathrm{sgn}\left(\frac{d\theta_n}{d\varphi}\right)\left|\frac{d\theta_n}{d\varphi}\right|^{\gamma}\right) \tag{3}$$

The diffusivity function can be then derived from Eq. (3)

$$D(\theta_n,t) = -\alpha t^{\alpha(1+\gamma)-1}\left(\frac{d\varphi}{d\theta_n}\right)^{\gamma}\int_{\theta_i}^{\theta_n}\varphi d\theta_n \tag{4}$$

Eq. (4) is a function depending on the normalized volumetric water content and time, and the time dependence of diffusivity can be eliminated if the relationship between Fickian and time exponents can be expressed as [62]

$$\gamma = \frac{1}{\alpha} - 1 \tag{5}$$

Substituting Eq. (5) into Eq. (4), yields that the diffusivity function purely depends on the volumetric water content

$$D(\theta_n) = -\alpha\left(\frac{d\phi}{d\theta_n}\right)^{\frac{1-\alpha}{\alpha}}\int_{\theta_i}^{\theta_n}\phi d\theta_n \tag{6}$$

By calculating the derivative on the $\theta_n-\varphi$ profiles and integral terms at specific values of the volumetric water content, the values of $D(\theta_n)$ can be obtained.

2.2. Diffusivity based on Lockington and Parlange model

According to the work of Lockington and Parlange [58], the diffusivity function $D(\theta_n)$ can be considered as a separate function of θ_n [mm^3mm^{-3}] and time t [sec]:

$$D(\theta_n) = 2\alpha t^{2\alpha-1}\delta(\theta_n) \tag{7}$$

where $\delta(\theta_n)$ [$mm^2\ s^{-1}$] is the hydraulic diffusivity, which is a function of θ_n only.

We take the wetting front position L to be a simple power of time t [sec]:

$$L = st^{\alpha} \tag{8}$$

where s [$mm\ s^{-1/2}$] is proportionality coefficient, which can be expressed as [76]:

$$s^2 = \int_0^1 (1+\theta_n)\delta(\theta_n)d\theta_n \tag{9}$$

Parlange et al. [77] and Campbell [78] proposed a power-law diffusivity equation. We took the dependence of $\delta(\theta_n)$ on θ_n to be a power-law

$$\delta(\theta_n) = D_0{\theta_n}^k \tag{10}$$

Substituting Eq. (10) into Eq. (9), the parameter D_0 can be direct obtained:

$$D_0 = \frac{s^2(k+1)(k+2)}{2k+3} \tag{11}$$

Substituting Eqs. (10) and (11) into Eq. (7), the diffusivity based on Lockington and Parlange model (L-P model) was obtained as:

$$D(\theta_n) = \frac{2\alpha t^{2\alpha-1}s^2(k+1)(k+2)}{2k+3}\theta_n^k \tag{12}$$

According to Lockington et al. [79], the parameter k will be suitable for the non-stationary media and they suggested a value of k=6. When the time exponent α is 0.50, the diffusion is independent of time t [sec].

2.3. Diffusivity based on Meyer and Warrick model

Meyer and Warrick [80] proposed an analytical solution for extracting unsaturated diffusivity function from the Boltzmann transformed data. When the effect of gravity was neglected and the initial water content in the specimen was assumed to be zero, the volumetric water content profile was expressed as a function of the normalized non-Boltzmann variable φ_n as follows:

$$\theta_n = \theta_s\frac{\varphi_m-\varphi_n}{\varphi_m-A\varphi_n} \tag{13}$$

where A is the shape factor. $\varphi_n=\varphi/\varphi_i$, φ_i is the value of φ when $\theta_n=0$. Moreover, Meyer and Warrick [80] introduced a method to build the unsaturated diffusivity function using θ_s and A as follows:

$$D(\theta_n) = \frac{\alpha(1-A)^{\gamma}\theta_s^{\gamma+1}\varphi_m^{\gamma+1}}{A(\theta_s-A\theta)^{2\gamma}}\cdot\left[\frac{1-A}{A}\log\left|1-A\frac{\theta}{\theta_s}\right|+\frac{\theta}{\theta_s}\right] \tag{14}$$

Abd and Milczarek [16] suggested that the Eq. (13) provides a very good fit to the data in the whole region of the φ_n variable except for the region of small θ_n. In order to analyze the unsaturated diffusivity in the region of small θ_n, a power law approximation was proposed:

$$\theta_n = \theta_0\left(1-\frac{\varphi_n}{\varphi_0}\right)^m \tag{15}$$

where θ_0 is the amplitude parameter, φ_0 is the limit value of the normalized non-Boltzmann variable, m is an exponent parameter. According to the Meyer and Warrick model (M-W model) [16], the approximate diffusivity function $D(\theta_n)$ was established by introducing a time exponent α:

$$D(\theta_n) = \alpha m^{(1-1/\alpha)}\varphi_0^{1/\alpha}\theta_0^{(2-1/\alpha)}\left[1-\frac{m}{m+1}\left(\frac{\theta_n}{\theta_0}\right)^{1/m}\right]\left(\frac{\theta_n}{\theta_0}\right)^{1+(1-m)(1-\alpha)/m\alpha} \tag{16}$$

Eq. (16) considers the time exponent α and further develops the M-W model. Eq. (6) is used to theoretically calculate the unsaturated diffusivity. The approximate unsaturated diffusivity is obtained by using Eqs. (12) and (16), respectively. By comparing the results calculated by Eqs. (6), (12) and (16), the adaptability of the L-P model and the developed M-W model can be evaluated.

3. Materials and methods

3.1. Specimen preparation and setup of experiment

To investigate the diffusivity during water transport in unsaturated cracked sandstone, a fine sandstone from Rong County, Sichuan Province, in southern China was tested. A cylindrical rock specimen (W1) was prepared with a diameter of 26.54 mm and a length of 60 mm. The specimen W1 appears homogeneous with no obvious flaws, as shown in Fig. 1(a). According to the analysis result of X-ray diffraction (XRD), the mineralogical composition of specimen W1 is as follows: Quartz (97.4%), Illite (0.988%), and Kaolinite (1.612%). The tested specimen W1 was fractured with a modified Brazilian test in an axial extensional mode [2]. The axial fracture was generated through the indirect tension apparatus by using a load frame of WDW-100E as shown in Fig. 1(b). During the fracture generation, compressive stress was gradually increased until the rock breaks and the fracture, parallel to the long axis of

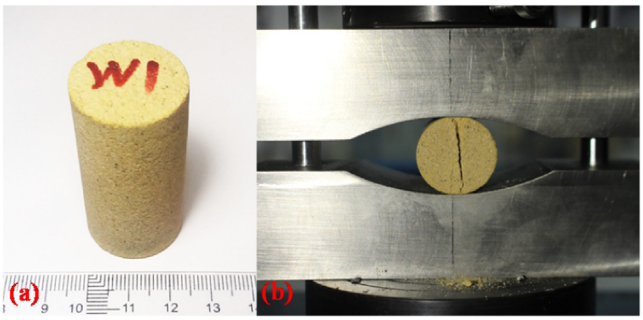

Fig. 1. Specimen investigated in the test. (a)The specimen is fine sandstone named W1. (b) The fractured specimen obtained by using modified Brazilian test.

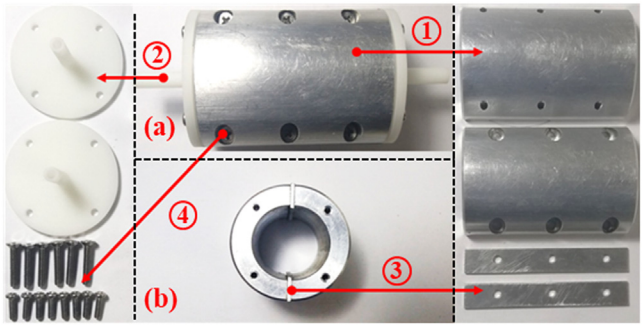

Fig. 2. Photograph of the core holder. The components of the core holder are: 1, aluminum semicircle wall with a diameter of 25.50 mm and a length of 60 mm; 2, end cap made of photosensitive resin; 3, rectangular aluminum sheet with a dimension of 60 mm × 8 mm × 1 mm; 4, screw spike. The front of the core holder is shown in (a), and the top view of the core holder without 2 in (b).

the specimen, extended throughout the entire length of the core. Prior to the experiment, the sandstone specimen was dried in an oven at 105°C for 24 h until the weight was constant.

A core holder, as shown in Fig. 2, was used to hold the specimen. The core holder has two aluminium semicircle walls with a diameter of 28 mm and a length of 60 mm. The end caps are made of photosensitive resin to keep the specimen stationary. The rectangular aluminium sheet with a dimension of 60 mm × 8 mm × 1 mm (length × width × height) was used to keep the width of crack. The screw spikes are applied in the connection and consolidation of each part of the core holder. Aluminium parts have low neutron attenuation properties which allow receiving better signals from the water present in the specimen domain.

3.2. Facility of neutron radiography

The neutron radiography experiments were performed at the cold neutron guide B located at guide hall of China Advanced Research Reactor (CARR) in the China Institute of Atomic Energy (CIAE). The neutron flux rate was set at 1.03 × 107 n/cm^2/s when the reactor operated at 20 MW power. The neutron imaging facility is located next to the end of the beam guide, and the ratio of the collimator tube length to its aperture diameter, L/D, is 85. The facility provides most neutrons between wavelengths of 0.8 and 10 Å (with a peak at 2.9 Å). The real-time detector system is equipped with a new scientific complementary metal oxide semiconductor (CMOS) camera with 5.5 million pixels and speed up to 100 fps at full frame as shown in Fig. 3(a). Neutron radiographs are obtained using the CMOS detector at a rate of 10 fps. The CMOS detector is equipped with a Li^6F/ZnS(Ag) scintillator and the field of view is 10 mm × 10 mm. The native spatial resolution of the detector is 100 μm determined by the pixel size of the Timepix readout. The neutron imaging facility provides images with much higher resolution and sensitivity at high frame rate, and more detailed technical parameters information has been reported by He et al. [95].

According to the XRD result, the main mineral composition of the specimen W1 is Quartz without the organic matter containing hydrogen. The effect of coherent scatting due to the quartz was not observed in previous work and hence the water imbibed into the sandstone W1 is deemed to be a primary cause leading to neutron scatter. Consequently, neutron radiography was selected as an effective research method to observe the wetting dynamics [9,18,50,81]. The schematic diagram of the experimental setup was shown in Fig. 3(b), and the exact steps of the experiment are as follows: (i) obtain 10 dark current images (shutter closed, no neutron illumination) and 10 flat field images (shutter opened without specimen) [81]; (ii) hang the specimen holder in front of the scintillator screen and fix the core holder on the specimen holder 10 mm away from the scintillator screen, as shown Fig. 3(c), then take 10 images of the dried specimen, denoted as $I_{(Dry)}$; (iii) keep the neutron beam open, and use a peristaltic pump to supply distilled water by silicone tube at the velocity of 5 ml/min until the base of the specimen contacts the free surface of the water, this moment is defined as baseline (zero) time [8]. The neutron images acquired after baseline time are denoted as $I_{(Wet)}$. The exposure time is 0.10 s for each raw neutron image. The experiment lasted 39.60 s and a total of 27 images were selected to calculate the diffusivity and the time interval is 1.50 s for the selected images.

3.3. Neutron image processing and water content calibration

The raw neutron images were processed by using *ImageJ* software [82,83], and all of them were processed to remove background noise, beam heterogeneities in the detector [18,51] and the effect of the dry sandstone speciment and the core hoder on the neutron intensity [50]:

$$I_w = \frac{I_{(Wet)} - I_{(DF)}}{I_{(Dry)} - I_{(DF)}} \tag{17}$$

where I_w is net water neutron images, $I_{(DF)}$ is the reference image of the Dark Field, which was acquired from the mentioned ten dark current images. $I_{(Dry)}$ is the dry image of the specimen or calibration cell, which was acquired from the median of the ten dry specimen images or ten dry calibration cell images [23]. More detailed information about the processing of neutron images has been reported in one previous publication by Zhao et al. [9].

Due to the interaction with the tested material, the neutrons can attenuate as the neutron beam (e.g., single wavelength) traversing an object [20,76], and this phenomenon can be characterized and quantified by Lambert-Beer law [84].

$$T/T_0 = \exp\left(-\eta\omega_t\right) \tag{18}$$

where T is the transmitted intensity, T_0 is the original intensity, η [mm^{-1}] is the attenuation coefficient of water, and ω_t [mm] is the time-dependent water thickness along the direction of neutron beam. According to Eq. (18), there is a linear relationship between $-\ln(T/T_0)$ and the time-dependent water thickness ω_t [mm]

$$-\ln\left(T/T_0\right) = \eta\omega_t \tag{19}$$

However, scattering effects were dynamically changeable with the increasing of water thickness, and the deviation was increased prominently due to scattering of water depending on the water thickness [32,46,85–87]. Therefore, Eq. (19) cannot be used to describe the attenuation behavior of neutron beam. In this study, we introduce an empirical correction parameter β [mm^{-2}] to correct

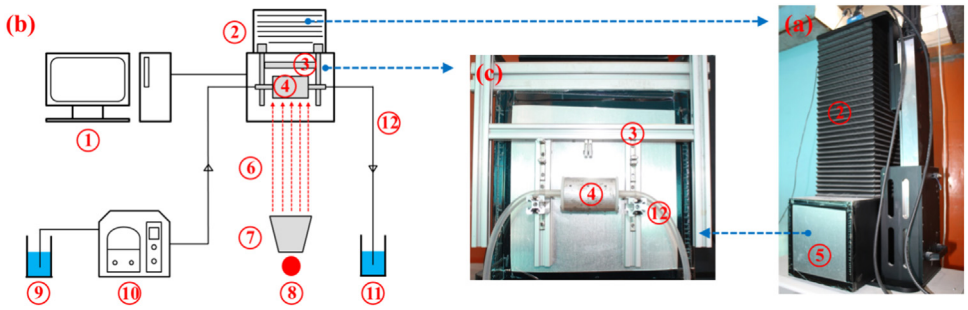

Fig. 3. Equipment layout of neutron radiography used to monitor water diffusivity during flow. (a) Neutron Imaging Facility; (b) Schematic diagram of the experimental setup; (c) Detailed position of the core holder in front of the detector. The components of the setup are: 1, Computer data acquisition system; 2, CMOS camera box; 3, Specimen holder; 4, Core holder; 5, Scintillator; 6, Neutron beam; 7, Collimator; 8, Source; 9, Water container; 10, Peristaltic pump; 11, Waste water collector; 12, Silicone tube.

the scattering and beam hardening effects by assuming following [86]:

$$\eta' = \beta\omega_t + \eta \tag{20}$$

where, η' [mm^{-1}] is an effective attenuation coefficient whose role is to convert transmission T/T_0 to the time-dependent water thickness ω_t [mm]. Combining Eqs. (19) and (20), we can obtain:

$$-\ln(T/T_0) = \beta\omega_t^2 + \eta\omega_t \tag{21}$$

The water thickness ω_t penetrated by neutron beam can be expressed as

$$\omega_t = -\eta/(2\beta) - \sqrt{(\eta/(2\beta))^2 - \frac{1}{\beta}\ln(T/T_0)} \tag{22}$$

The value of the attenuation coefficient η and correction coefficient β is 0.4419 mm^{-1} and 0.0463 mm^{-2}, respectively, and both of them have been reported by Zhao et al. [9]. The value of T/T_0 can be obtained by measure the region of interest (ROI) of the net water image. A net water image of specimen W1 at the time of 9.0 s was selected to illustrate the process of measurement, as shown in Fig. 4(a). From Fig. 4(a), it shows that the selected net water image was covered by 9.0 mm^2 red grids and divided into 6 regions (yellow dash line) with the grid as reference, and then a rectangle area was selected in each region as ROI and marked with a solid blue line. The average net water transmission profiles along the vertical direction of the specimen were extracted from the images. Thus, applying Eq. (22), the volumetric water content θ [mm^3mm^{-3}] can be calculated as:

$$\theta = \frac{\omega_t}{2\sqrt{r^2 - h^2}} \tag{23}$$

where r [mm] is the radius of the core and h [mm] is the distance from the center of the specimen to the pixel. Due to the diffusivity of water, the wetting front continuously moves forward, and the volumetric water content reaches the lowest at the leading edge of the wetting front. The transmission increases with the decreasing of volumetric water content in the direction of the water diffusivity, and the specimen W1 is assumed to be dry (i.e., θ=0) when the value of the transmission is equal to or exceeds a threshold value. The threshold value for specimen W1 is 1.00 based on the average transmission value of the dry image. The positions of wetting front in monitoring ROI 2-1 and ROI 2-2 are shown in Fig. 4(b).

4. Results and discussion

The images regarding the water diffusivity process in cracked sandstone were obtained by using dynamic neutron radiography. According to the neutron images, the normalized volumetric water content distributions in every monitoring ROI (1-1, 1-2, 2-1, 2-2, 3-1, 3-2) of the specimen were analyzed. The wetting front position L and the normalized volumetric water content along the vertical direction of each ROI were extracted at various time step of the experiment. The initial region of ~5mm from the crack surface to the white short dot line as shown in Fig. 4(a) of the ROI was cropped for the analysis because the surface diffusivity of water can potentially influence the distribution of water content at this region [16]. According to classical theories of the water imbibition in porous media [17], the relationship between the wetting front position and the square root of the time can be expressed as $L = st^{0.5}$. Some scholars believed that the classical theory cannot properly and accurately model the experimental phenomena of anomalous diffusivity. They thought that the wetting front propagation follows the formula $L = st^{\alpha}$ [88,89]. Based on the experimental data in ROI, the double logarithmic plots of the wetting front position *versus* time and the fitted lines of them are presented in Fig. 5(a)–(c). The fitted curves are in good agreement with the experimental data. It shows a clearly non-classical (i.e., $a \neq 0.5$) behavior of the wetting front diffusivity, which was classified as non-Boltzmann phenomenon [16]. The values of the regressed parameters were listed in Table 1. The relative errors of the time exponent α in ROIs 1-1 and 1-2, ROIs 2-1 and 2-2, and ROIs 3-1 and 3-2 are 15.79%, 10.53% and 16.28%, respectively. The plots of the wetting front position L against t^{α} are shown in Fig. 6. From Fig. 6, it is apparent that the regressed model well agrees with the experimental data with all R^2 values exceeding 0.99. The values of the regressed parameters were given in Table 2.

Table 1
The fitting parameters time exponent (α), intercept (b) and goodness of fit (R^2) for ROI of the specimen.

Monitoring ROI	α	b	R^2
1-1	0.33	1.30	0.998
1-2	0.32	1.31	0.998
2-1	0.34	1.21	0.998
2-2	0.34	1.28	0.998
3-1	0.37	1.18	0.999
3-2	0.36	1.19	0.999

Table 2
The fitting parameters proportionality coefficient (s) and goodness of fit (R^2) for ROI of the specimen.

Monitoring ROI	α	s	R^2
1-1	0.33	3.68	0.998
1-2	0.32	3.70	0.998
2-1	0.34	3.41	0.998
2-2	0.34	3.60	0.996
3-1	0.37	3.31	0.998
3-2	0.36	3.27	0.998

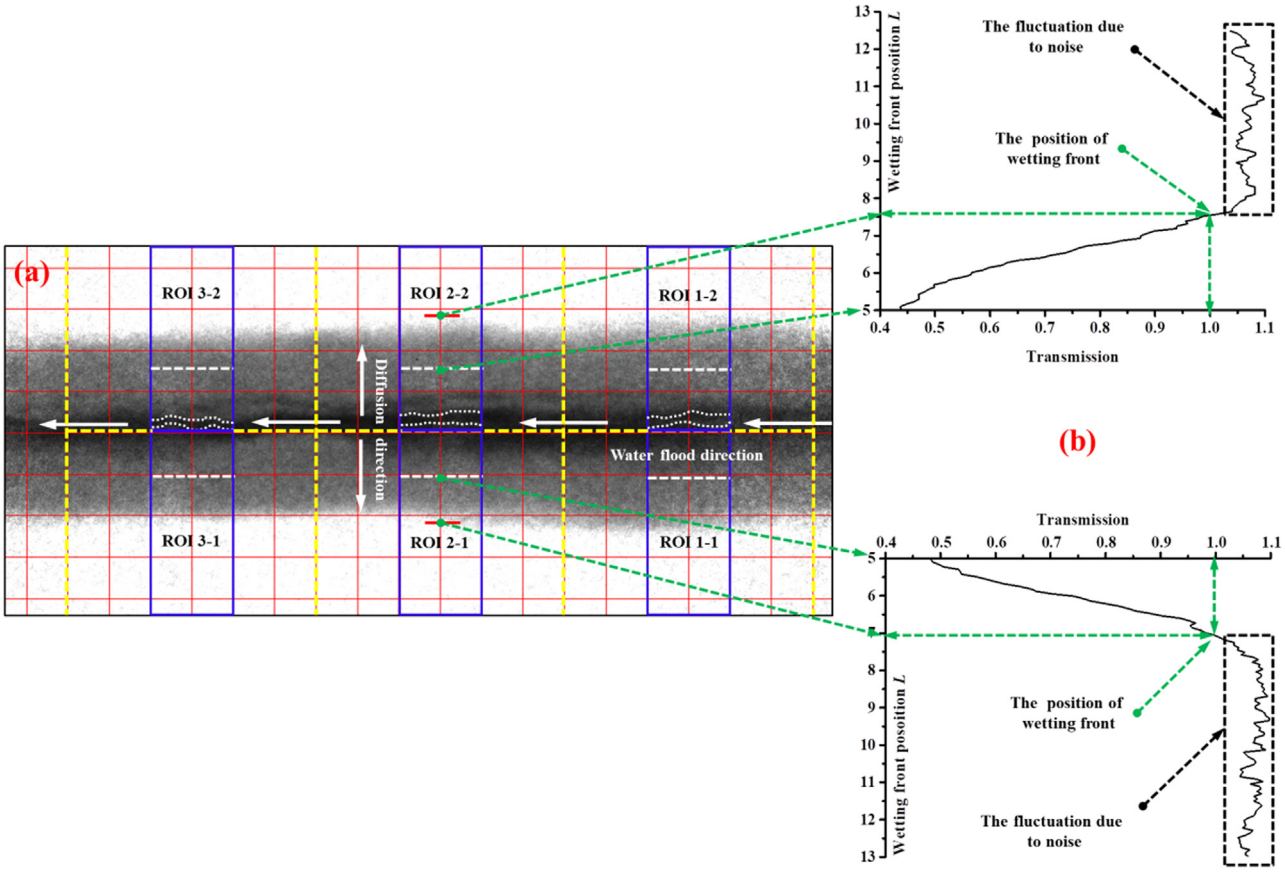

Fig. 4. Schematic of the method for defining the wetting front position L in ROI of cracked sandstone. (a) The typical image of net water at 4.50 s and the positions of the monitoring ROI. (b) The distribution of the transmission and the wetting position L in ROIs 2-1 and 2-2 at 4.50 s.

The anomalous diffusivity phenomenon may be caused by these factors including the roughness fracture interface, anisotropy and heterogeneity of matrix, forced hydrodynamic pressure, hydrostatic pressure, insufficient water source and nonuniform boundary condition. The rough fracture interface only exerts an influence on the initial diffusivity of matrix near the fractured areas. However, the study complete avoids the initial diffusivity state near the fractured zone, and hence the effect of rough interface can be ignored. The forced hydrodynamic pressure is applied to the fractured specimen through the peristaltic pump, and its influence is eliminated due to very low force. Under the current conditions of experimental scale, the specimen only with a few centimeters cannot cause high gravity head compared with strong capillary pressure [90], ignoring the influence of hydrostatic pressure. In our research, all the obtained time exponents by hydraulic diffusivity in three ROIs are close to 0.32, which is in agreement with the result derived by Li and Zhao [91] considering the Berea sandstone matrix heterogeneity and introducing the 3-D fractal dimension in the time exponent. Additionally, our time exponents are in the range from 0.25 to 0.5, which is analogous to values calculated by the fractal imbibition theoretical models considering the matrix anisotropy characterized by 2-D fractal dimension of tortuous streamlines [56,89]. Therefore, the micro heterogeneity and anisotropy of sandstone matrix may be a prominent factor leading to anomalous diffusivity phenomenon, although our sample appearing macro homogeneous. Moreover, different from previous experimental condition, the wetting cross-section gradually varies from the radius to zero with nonuniform geometric boundary. Thus, the vertical wetting front monitored by 1-D neutron radiography may be longest distance along the imbibition direction when the fronts near the boundary already reach the equilibrium state. Although the shape of wetting front cannot be observed in the 3-D space due to the limitation of neutron radiography, we infer that the complicated 3-D hydraulic transport due to varying geometric boundary leads to the observed 1-D anomalous diffusivity from longitudinal protection cross-section. Finally, the water content diffusing from narrow fracture space to matrix is different from the standard imbibition experiment, which results in the insufficient water source supplying for matrix imbibition, hence generating an anomalous diffusivity phenomenon deviating from the existing standard absorption.

The results of the normalized volumetric water content profiles along the monitoring lines of each ROI with a time interval of 1.50 s from the beginning of water imbibition were shown in Fig. 7(a)–(f). Fig. 8(a)–(f) show the correlation between the normalized volumetric water content θ_n and φ at different times of water diffusivity. Except for some data sets obtained at the beginning of the experiment in monitoring ROI 1-1, all of the profiles generally converge into a master curve, which intercepts the abscissa axis at 3.625φ. The abscissa intercepts of others ROI (1-2, 2-1, 2-2, 3-1, 3-2) are 3.750φ, 3.406φ, 3.625φ, 3.250φ and 3.250φ, respectively. Based on the values of abscissa intercept, the average value φ_i for each ROI was 3.625, 3.750, 3.406, 3.625, 3.250 and 3.250, respectively. For each ROI, the correlation between the normalized volumetric water content θ_n and the normalized non-Boltzmann variable φ_n was further plotted in Fig. 9(a)–(f), respectively.

In order to study the diffusivity of unsaturated cracked sandstone specimen, three methods were employed. In method (i), an diffusivity function, Eq. (6), was derived based on Generalized Fickian law. The derivative and integral terms of the Eq. (6) were calculated at specific values of the normalized water content, which

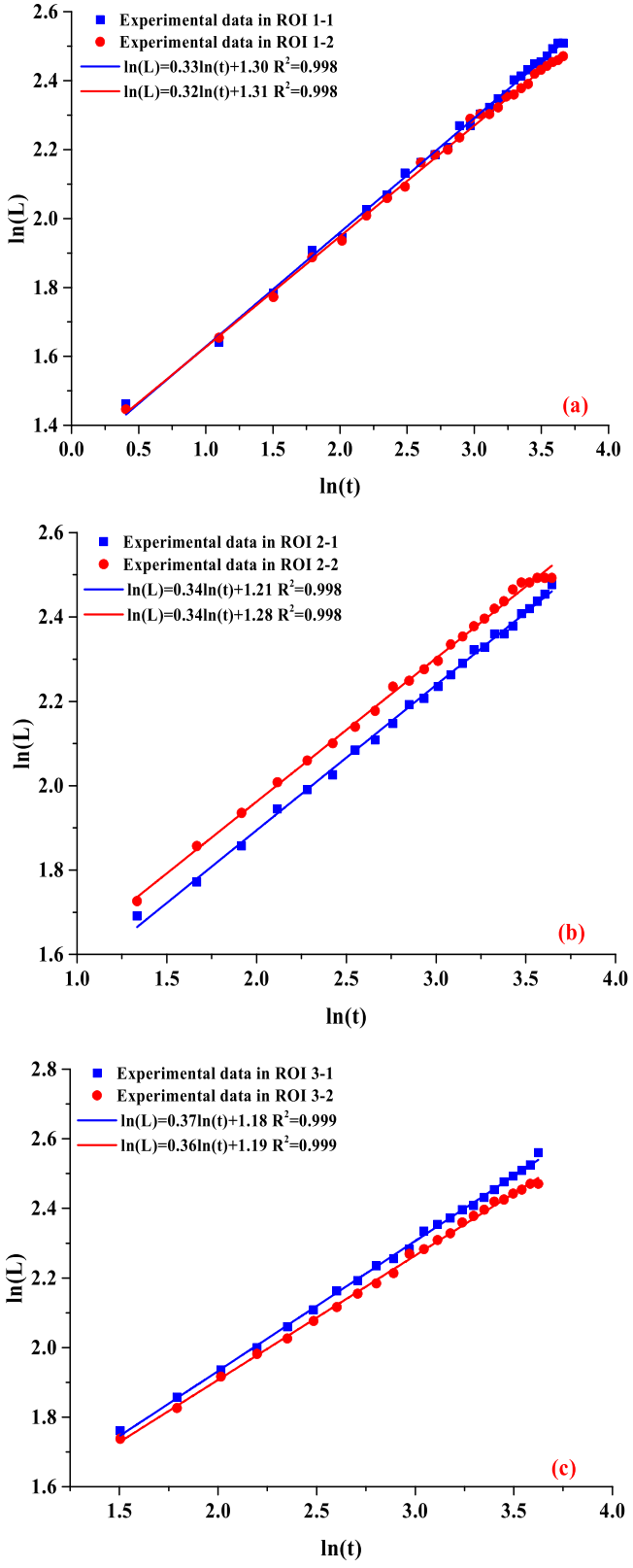

Fig. 5. The double logarithmic plot of the wetting front position versus time for ROI of cracked sandstone, (a) ROI 1-1 and ROI 1-2, (b) ROI 2-1 and ROI 2-2, (c) ROI 3-1 and ROI 3-2 of cracked sandstone.

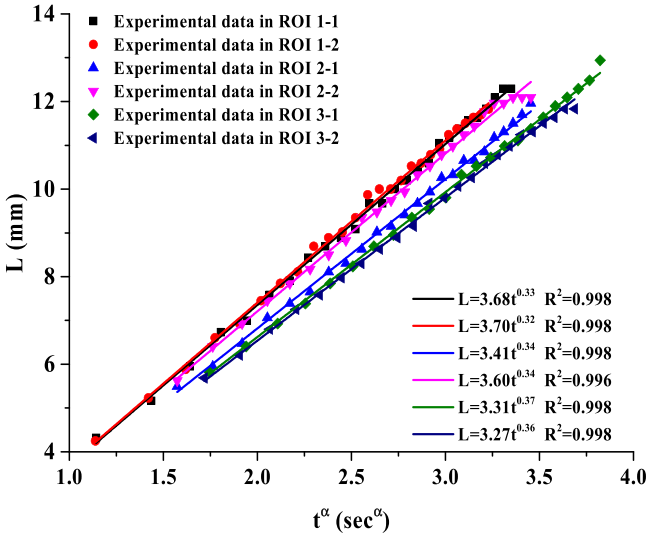

Fig. 6. The plot of wetting front position L versus the power law of time t^{α} for ROI of the specimen.

Table 3
The fitting parameters amplitude parameter (θ_0), limit value of the normalized non-Boltzmann variable (φ_0), exponent parameter (m) and goodness of fit (R^2) for ROI of the specimen.

Monitoring ROI	θ_0	φ_0	m	R^2
1-1	1.43	0.97	0.33	0.870
1-2	1.62	0.96	0.41	0.918
2-1	1.54	0.96	0.35	0.891
2-2	1.59	0.97	0.33	0.897
3-1	1.42	0.97	0.25	0.875
3-2	1.59	0.98	0.37	0.913

can refer to the $\theta_n - \varphi$ profile curves shown in Fig. 8(a)–(f). Then the scatter data of the diffusivity was further obtained. In method (ii), the other diffusivity function, Eq. (12), was obtained according to L-P model. The diffusivity was calculated using Eq. (12). In method (iii), the finally diffusivity function, Eq. (16), was proposed based on M-W model. The related parameters were obtained by fitting the experimental data, as shown in Fig. 9(a)–(f). The regression parameters were listed in Table 3. Then, the diffusivity was re-obtained by using Eq. (16).

The relationship between the diffusivity $D(\theta_n)$ in log scale unit and the normalized water content θ_n for ROIs of the specimen were illustrated in Fig. 10(a)–(f). Whichever ROI and/or model was used, the value of the diffusivity increases non-linearly with the increase of normalized water content. This growth spanned several orders of magnitude (i.e., from 10^{-12} to 10 $mm^2\ s^{-1}$ in Fig. 10(a)). At the low water content, the diffusivity of all ROIs did not reduce with the increase of water contents as shown in Fig. 10(a)–(f), which is the same with the results for fired clay brick and sandstone reported by Abd and Milczarek [16] and Zhao et al. [9], but different from the results for calcium silicate brick reported by Carmeliet et al. [92].

The black scattered points in Fig. 10(a)–(f) represented the diffusivity obtained by the Generalized Fickian law. The discretization of these black points is caused by the scattering $\theta_n - \varphi$ profiles [9,93]. The distribution of scattered points near the saturated water content (i.e., θ_n=1.0 mm^3mm^{-3}) is most intensive, as shown in the red dashed box selection areas in Fig. 10(a)–(f). This phenomenon may be due to that the pores in the rock specimen are constantly filled with water, and more and more of them reach near saturation. The short-dash lines in Fig. 10(a)–(f) represented the diffusivity obtained by the L-P model. Short-dash lines of dif-

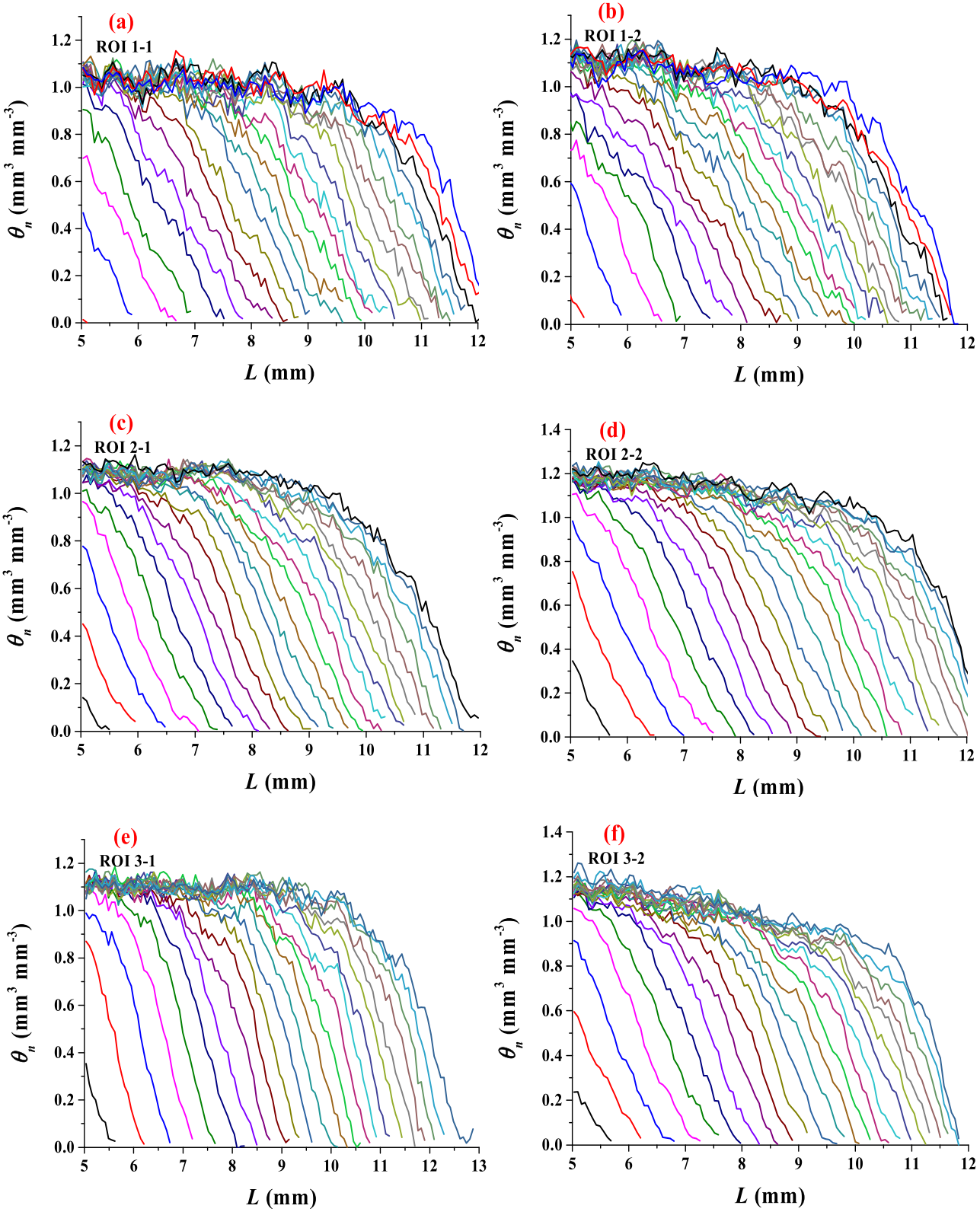

Fig. 7. The normalized volumetric water content profile along the monitoring ROI of cracked sandstone with a time interval of 1.50 s, (a) ROI 1-1, (b) ROI 1-2, (c) ROI 2-1, (d) ROI 2-2, (e) ROI 3-1, (f) ROI 3-2.

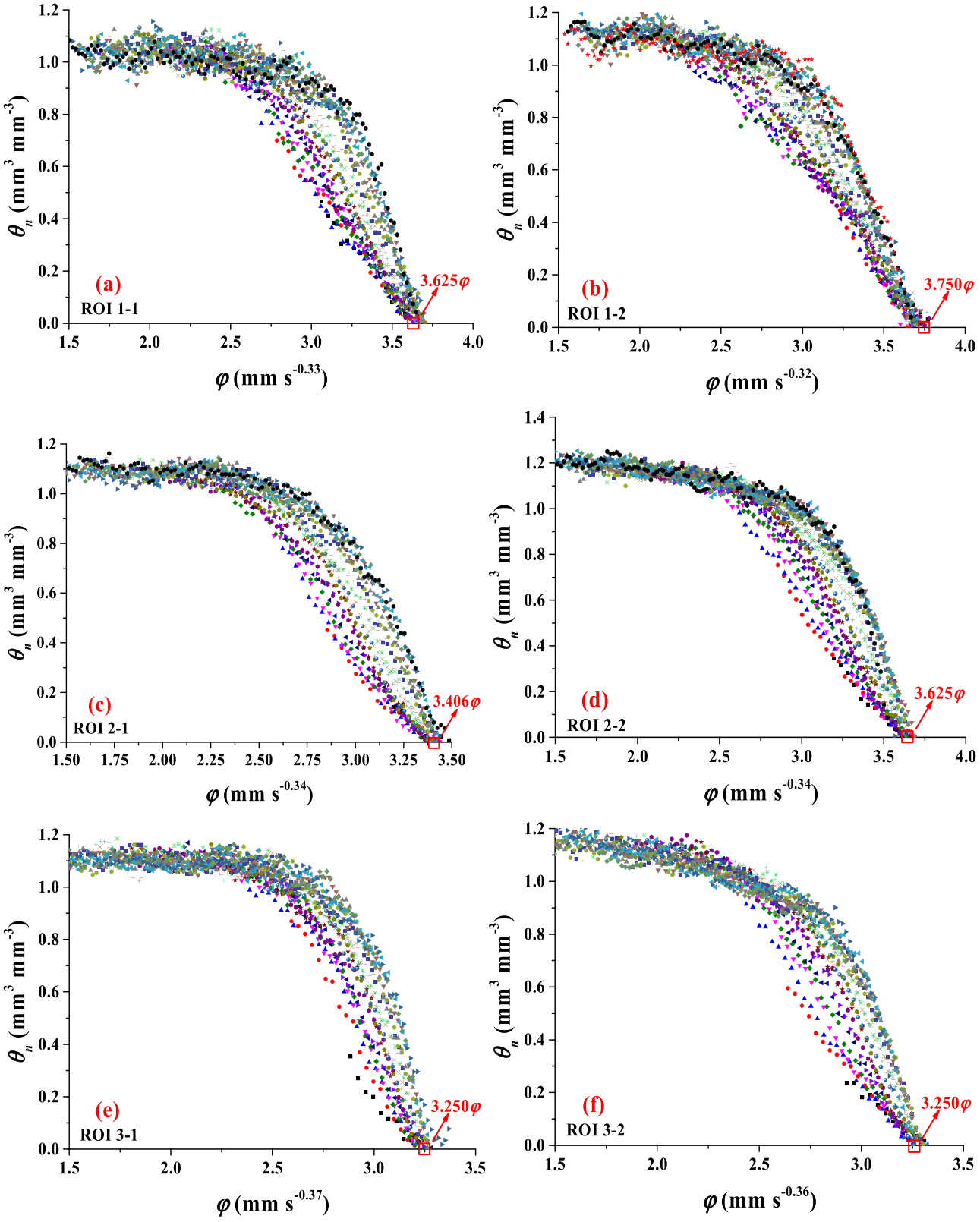

Fig. 8. Profiles of the volumetric water content versus the non-Boltzmann variable for ROI of cracked sandstone, (a) ROI 1-1, (b) ROI 1-2, (c) ROI 2-1, (d) ROI 2-2, (e) ROI 3-1, (f) ROI 3-2.

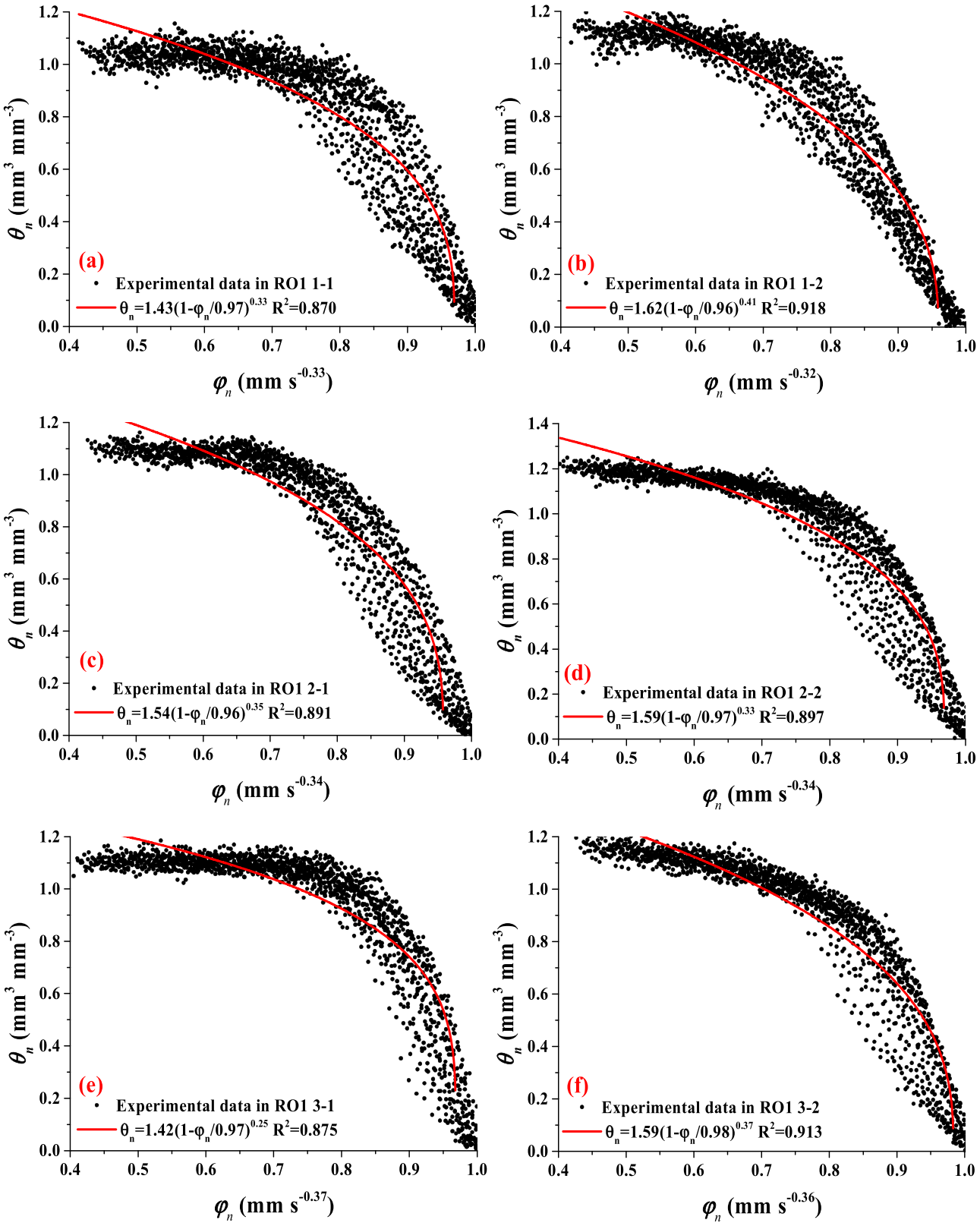

Fig. 9. Profiles of the normalized volumetric water content versus the normalized non-Boltzmann variable for ROI of cracked sandstone, (a) ROI 1-1, (b) ROI 1-2, (c) ROI 2-1, (d) ROI 2-2, (e) ROI 3-1, (f) ROI 3-2.

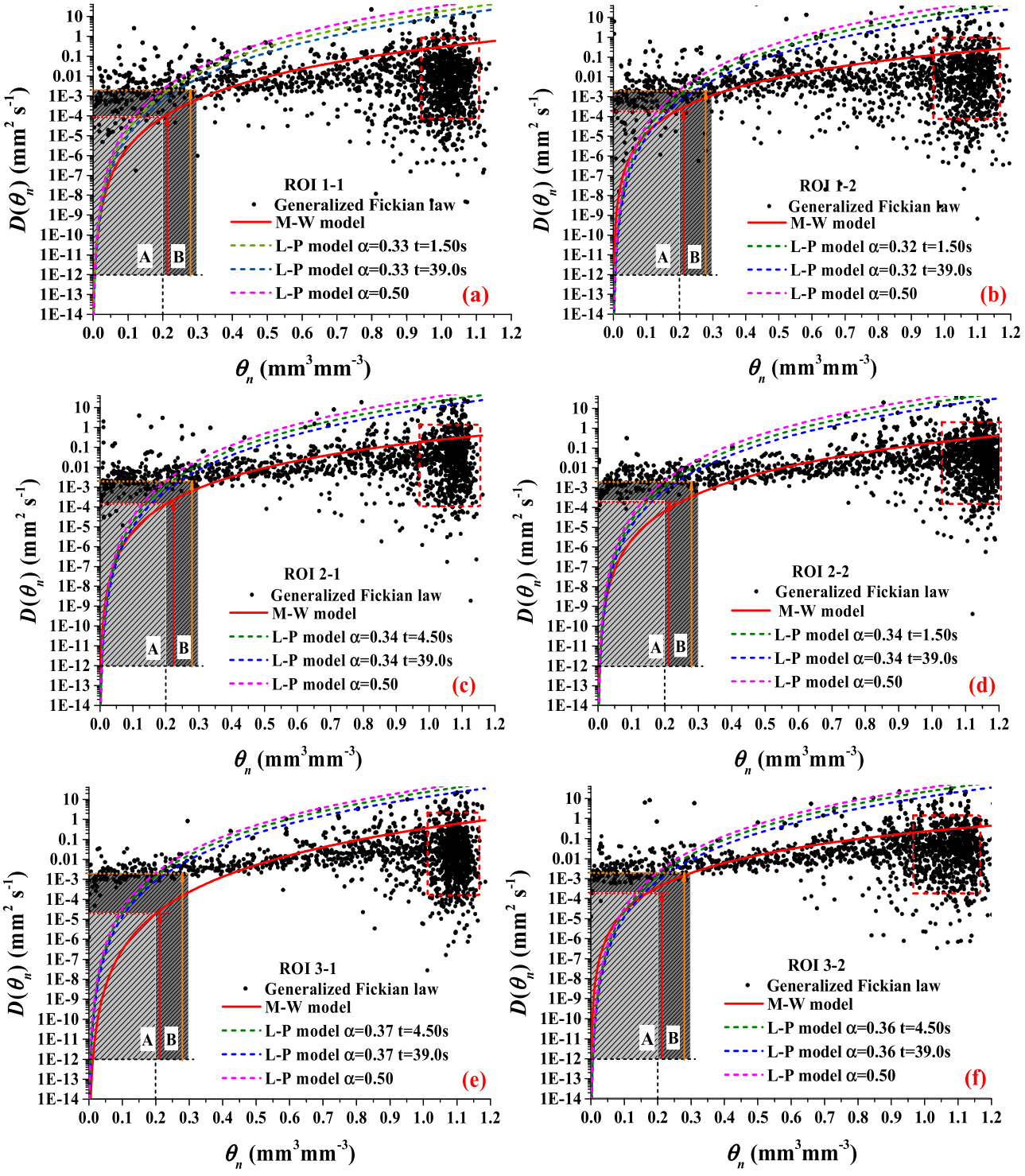

Fig. 10. The anomalous diffusivity calculated by three methods shown in log scale units versus the normalized volumetric water content for ROI of cracked sandstone, (a) ROI 1-1, (b) ROI 1-2, (c) ROI 2-1, (d) ROI 2-2, (e) ROI 3-1, (f) ROI 3-2. The scattering points were calculated based on Generalized Fickian law. The short-dash lines were obtained according to L-P model (the olive and blue short-dash lines represent the anomalous diffusivity in initial and final time respectively, when the time exponent is not 0.50, and the orange short-dash line represents the anomalous diffusivity, when the time exponent is 0.50). The red solid line was obtained by the developed M-W model.

ferent colors represent the diffusivity obtained under different calculation conditions. According to L-P model, the diffusivity is independent of time under the condition α=0.50, as the pink short-dash line shown in Fig. 10(a)–(f). When the time exponent is not 0.50, the diffusivity was influenced by time. In order to obtain the range of influence of time on the diffusivity, the initial and final times of spontaneous imbibition in each ROI were selected to calculate, as the olive and blue short-dash lines shown in Fig. 10(a)–(f). Values of the diffusivity for the three short-dash lines are almost the same with increasing normalized water content from 0 to 0.05 mm^{3}mm^{-3}, as shown in Fig. 10(a)–(f). Some small deviations were appeared between the three short-dash lines at the vertical axis direction, which increase slowly with increasing normalized water content from 0.05 to 0.20 mm^{3}mm^{-3}. Then, these

deviations kept almost constant. The dependence of the diffusivity calculated by the L-P model on the time is not significant, especially at low water content area (e.g., θ_n<0.05 mm^3mm^{-3}).

The red solid lines in Fig. 10(a)–(f) represented the diffusivity obtained by the developed M-W model. It can be found that the diffusivity calculated by the developed M-W model increase rapidly with increasing normalized water content from 0 to 0.2 mm^3mm^{-3}, which is almost the same as that calculated by L-P model, as the rectangular shadow regions A and B shown in Fig. 10(a)–(f). Take ROI 1-1 as an example, the diffusivity calculated by the developed M-W (or L-P) model grew from 10^{-12} to 10^{-4} mm^2 s^{-1} (10^{-12} to 10^{-3} mm^2 s^{-1}) with increasing normalized water content from 0 to 0.2 mm^3mm^{-3}, as the rectangular shadow region A (B) shown in Fig. 10(a). This phenomenon is consistent with the results reported by Kang et al. [18], but different from Carmeliet et al. [92]. The minimum value of the diffusivity appeared in the vicinity of zero water content, which is different from the results for fired clay brick reported by Abd and Milczarek [16], and in their studies the minimum value of the diffusivity disappeared in the vicinity of zero water content. This difference may be attributed to different materials tested in the experiments [16].

The increasing trend of the diffusivity calculated by L-P model and the developed M-W model tend to be flat, when the normalized water content is larger than 0.2 mm^3mm^{-3}. This phenomenon is different from the results for concrete, clay brick and silty sandstone reported by Nizovtsev et al. [94], Abd and Milczarek [16,17] and Zhao et al. [9], respectively. In their reports, the growth rate of diffusivity kept almost constant but the rate speeded up once the water content reached near saturation, which may be due to more water being filled in pores, hence intensifying the water transfer under capillary forces [9,94]. The diffusivity predicted by the developed M-W model was in a good agreement with the scattered points obtained by the Generalized Fickian law under the condition that the normalized water content is larger than 0.2 mm^3mm^{-3}, as shown in Fig. 10(a)–(f). Compared with the developed M-W model, the diffusivity of sandstone specimen is obviously overestimated by L-P model with normalized water content larger than 0.2 mm^3mm^{-3}, as shown in Fig. 10(a)–(f). This overestimation may be resulted from the relative stability of pore space after water imbibition due to the low contents of clay minerals, such as Illite (0.988%), Kaolinite (1.612%) within the tested specimen.

In summary, all three methods can be used to describe the diffusivity in the cracked sandstone with homogeneous pore structure. The diffusivity obtained in different ROIs are different to some extent, which may be due to the different contact time between water and rock crack surface caused by different surface roughness of each ROI. The diffusivity calculated by the developed M-W model is closest to that obtained by the Generalized Fickian law, which suggests that the developed M-W model can better describe the diffusivity based on non-Boltzmann scaling. However, further studies are also necessary to evaluate the validity of the developed M-W model calculating the diffusivity for more types of specimens.

5. Conclusions

In this study, the dynamic process of water diffusivity from crack to unsaturated sandstone matrix is visualized in real time by neutron radiography. A correction coefficient was introduced in Lambert-Beer law to correct neutron scattering and beam hardening, so as to obtain reliable water content distribution from neutron images. According to these neutron images, the wetting front position along the axial direction of each ROI was extracted at various times. We discovered that the evolution of the wetting front over time obeys to non-Boltzmann transformation relationship. The impossible factors leading to the anomalous hydraulic diffusivity are anisotropy and heterogeneity of matrix, forced hydrodynamic pressure, hydrostatic pressure, insufficient water source and nonuniform boundary condition. The anisotropy and heterogeneity of matrix and nonuniform geometric boundary are mainly expected to exert significant influence on the anomalous diffusivity phenomenon. Additionally, the insufficient water source due to nonstandard imbibition experiment, including the rough fracture interface and narrow fracture channel is subordinate factor.

The diffusivity was determined by three models including Generalized Fickian law, L-P model and the developed W-M model. No matter which ROI and/or model was used, the value of the diffusivity increases non-linearly over several orders of magnitude (i.e., from 10^{-12} to 10 mm^2 s^{-1}) with the increase of normalized water content. The diffusivity calculated by the developed M-W model increase rapidly with increasing normalized water content from 0 to 0.2 mm^3mm^{-3}, which is almost the same as that calculated by L-P model. When the normalized water content is larger than 0.2 mm^3mm^{-3}, the increasing trend of the diffusivity calculated by L-P model and the developed M-W model tend to be flat. Compared with the developed M-W model, L-P model obviously overestimated the diffusivity. This overestimation may be resulted from the relative stability of pore space after water absorption due to the low contents of clay minerals within the tested specimen. The diffusivity calculated by the developed M-W model is closest to that obtained by the Generalized Fickian law when the normalized water content is larger than 0.2 mm^3mm^{-3}. It means that the developed M-W model can better describe the anomalous diffusivity phenomenon on non-Boltzmann scaling.

Moreover, the successful application of neutron radiography in real-time monitoring of the diffusion process of water in cracked sandstone offers a feasible and more reliable way for characterizing fluid migration in others porous media material. The developed W-M model, which consider the time exponent, also provides a convenient manner to quantitatively define and model the diffusivity.

Declaration of Competing Interest

The authors declare that they have no known competing financial interests or personal relationships that could have appeared to influence the work reported in this paper.

CRediT authorship contribution statement

Yixin Zhao: Methodology, Conceptualization, Validation. **Yang Wu:** Investigation. **Chuanlong Dong:** Software, Data curation. **Songbai Han:** Resources, Formal analysis. **Derek Elsworth:** Visualization. **Linfeng He:** Writing – review & editing, Writing – original draft.

Acknowledgments

The results presented in this article rely on the data collected at the Neutron Scattering Laboratory, China Institute of Atomic Energy. The China Institute of Atomic Energy is gratefully acknowledged for their support of this work and for providing access to the neutron imaging facility. This research is supported by the National Natural Science Foundation of China (Nos. 51861145403, 51874312, U1910206), Science and Technology Plant Project of Inner Mongolia Autonomous Region (No. 2019GG140), and Major Scientific and Technological Innovation Project in Shandong Province (Nos. 2019SDZY01, 2019SDZY02).

References

[1] S. Akin, A.R. Kovscek, Imbibition studies of low-permeability porous media, in: Proceedings of the SPE Western Regional Meeting, 26-27, Anchorage, Alaska, 1999, p. 54590, doi:10.2118/54590-MS.

[2] Z.T. Karpyn, A. Alajmi, F. Radaelli, P.M. Halleck, A.S. Grader, X-ray CT and hydraulic evidence for a relationship between fracture conductivity and adjacent matrix porosity, Eng. Geol. 103 (2009) 139–145, doi:10.1016/j.enggeo.2008.06.017.

[3] K. Li, R.N. Horne, Characterization of spontaneous water imbibition into gas-saturated rocks, SPE J. 6 (2001) 375–384, doi:10.2118/74703-PA.

[4] F. Doster, J.M. Nordbotten, M.A. Celia, Impact of capillary hysteresis and trapping on vertically integrated models for CO_2 storage, Adv. Water Resour. 62 (2013) 465–474, doi:10.1016/j.advwatres.2013.09.005.

[5] A.L. Herring, E.J. Harper, L. Andersson, A. Sheppard, B.K. Bay, D. Wildenschild, Effect of fluid topology on residual nonwetting phase trapping: implications for geologic CO_2 sequestration, Adv. Water Resour. 62 (2013) 47–58, doi:10.1016/j.advwatres.2013.09.015.

[6] A.F.B. Tompson, G.B. Hudson, D.K. Smith, J.R. Hunt, Analysis of radionuclide migration through a 200-m Vadose zone following a 16-year infiltration event, Adv. Water Resour. 29 (2006) 281–292, doi:10.1016/j.advwatres.2005.02.015.

[7] S.W. Wheatcraft, &S.W. Tyler, An explanation of scale-dependent dispersivity in heterogeneous aquifers using concepts of fractal geometry, Water Resour. Res. 24 (1988) 566–578, doi:10.1029/WR024i004p00566.

[8] C.L. Cheng, E. Perfect, B. Donnelly, H.Z. Bilheux, A.S. Tremsin, L.D. Mckay, L.D. Distefano, J.C. Cai, L.J. Santodonato, Rapid imbibition of water in fractures within unsaturated sedimentary rock, Adv. Water Resour. 77 (2015) 82–89, doi:10.1016/j.advwatres.2015.01.010.

[9] Y. Zhao, S. Xue, S. Han, L. He, Z. Chen, Characterization of unsaturated diffusivity of tight sandstones using neutron radiography, Int. J. Heat Mass Transf. 124 (2018) 693–705, doi:10.1016/j.ijheatmasstransfer.2018.03.090.

[10] D. Benavente, C. Pla, N. Cueto, S. Galvañ, J. Martínez-Martínez, M.A. García-del-Cura, S. Ordóñez, Predicting water permeability in sedimentary rocks from capillary imbibition and pore structure, Eng. Geol. 195 (2015) 301–311.

[11] M.Q. Hu, P. Persoff, J.S.Y. Wang, Laboratory measurement of water imbibition into low-permeability welded tuff, J. Hydrol. 242 (2001) 64–78.

[12] R.J. Gummerson, C. Hall, W.D. Hoff, Unsaturated water flow within porous materials observed by NMR imaging, Nature 281 (1997) 56–57.

[13] C. Leech, D. Lockington, Unsaturated diffusivity functions for concrete derived from NMR images, Mater. Struct. 36 (2003) 413–418.

[14] Z.T. Karpyn, P.M. Halleck, A.S. Grader, An experimental study of spontaneous imbibition in fractured sandstone with contrasting sedimentary layers, J. Petrol. Sci. Eng. 67 (2009) 48–56, doi:10.1016/j.petrol.2009.02.014.

[15] S. Roels, J. Carmeliet, Analysis of moisture flow in porous materials using microfocus X-ray radiography, Int. J. Heat Mass Transf. 49 (2006) 4762–4772, doi:10.1016/j.ijheatmasstransfer.2006.06.035.

[16] A. El Abd, J.J. Milczarek, Neutron radiography study of water absorption in porous building materials: anomalous diffusion analysis, J. Phys. D Appl. Phys. 37 (2004) 2305–2313, doi:10.1088/0022-3727/37/16/013.

[17] A. El Abd, A. Czachor, J.J. Milczarek, Neutron radiography determination of water diffusivity in fired clay brick, Appl. Radiat. Isot. 67 (2009) 556–559, doi:10.1016/j.apradiso.2008.11.014.

[18] M. Kang, E. Perfect, C.L. Cheng, H.Z. Bilheux, M. Gragg, D.M. Wright, J.M. Lamanna, J. Horita, J.M. Warren, Diffusivity and sorpvity of berea sandstone determined using neutron radiography, Vadose Zone J. 12 (2013) 1712–1717, doi:10.2136/vzj2012.0135.

[19] E. Perfect, C.L. Cheng, C.L. Kang, H.Z. Bilheux, H.Z. Lamanna, M.J. Gragg, D.M. Wright, Neutron imaging of hydrogen-rich fluids in geomaterials and engineered porous media: a review, Earth-Sci. Rev. 129 (2014) 120–135, doi:10.1016/j.earscirev.2013.11.012.

[20] M.A. Boone, T. De Kock, T. Bultreys, G. De Schutter, P. Vontobel, L. Van Hoorebeke, V. Cnudde, 3D mapping of water in oolithic limestone at atmospheric and vacuum saturation using X-ray micro-CT differential imaging, Mater. Charact. 97 (2014) 150–160, doi:10.1016/j.matchar.2014.09.010.

[21] S.V. Galkin, A.A. Efimov, S.N. Krivoshchekov, Y.V. Savitskiy, S.S. Cherepanov, X-ray tomography in petrophysical studies of core samples from oil and gas fields, Russ. Geol. Geophys. 56 (2015) 782–792, doi:10.1016/j.rgg.2015.04.009.

[22] M.G. Basavaraj, G.S. Gupta, New calibration technique for x-ray absorption studies in single and multiphase flows in packed bed, ISIJ Int. 44 (2004) 50–58.

[23] F.H. Kim, M. Asce, D. Penumadu, J. Gregor, N. Kardjilov, I. Manke, High-resolution neutron and x-ray imaging of granular materials, J. Geotech. Geoenviron. 139 (2013) 715–723.

[24] Q. Chen, M.K. Gingras, B. Balcom, A magnetic resonance study of pore filling processes during spontaneous imbibition in Berea sandstone, J. Chem. Phys. 119 (2003) 9609–9616, doi:10.1063/1.1615757.

[25] L.D. Hall, M.H.G. Amin, E. Dougherty, M. Sanda, J. Votrubova, K.S. Richards, R.J. Chorley, M. Cislerova, MR properties of water in saturated soils and resulting loss of MRI signal in water content detection at 2 tesla, Geoderma 80 (1997) 431–448.

[26] L. Pel, A.A.J. Ketelaars, O.C.G. Adan, A.A. Van Well, Determination of moisture diffusivity in porous media using scanning neutron radiography, Int. J. Heat Mass Transf. 36 (1993) 1261–1267.

[27] V. Cnudde, M. Dierick, J. Vlassenbroeck, B. Masschaele, B. Lehmann, P. Jacobs, L. Van Hoorebeke, Determination of the impregnation depth of siloxanes and ethylsilicates in porous material by neutron radiography, J. Cult. Herit. 8 (2007) 331–338, doi:10.1016/j.culher.2007.08.001.

[28] M.R. Deinert, J.Y. Parlange, T. Steenhuis, J. Throop, K. Ünlü, K.B. Cady, Measurement of fluid contents and wetting front profiles by real-time neutron radiography, J. Hydrol. 290 (2004) 192–201, doi:10.1016/j.jhydrol.2003.11.018.

[29] A.E.-G. El Abd, A. Czachor, J.J. Milczarek, J. Pogorzelski, Neutron radiography studies of water migration in construction porous materials, IEEE Trans. Nucl. Sci. 52 (2005) 299–304, doi:10.1109/TNS.2005.843642.

[30] R. Hassanein, H.O. Meyer, A. Carminati, M. Estermann, E. Lehmann, P. Vontobel, Investigation of water imbibition in porous stone by thermal neutron radiography, J. Phys. D Appl. Phys. 39 (2006) 4284–4291, doi:10.1088/0022-3727/39/19/023.

[31] P. Zhang, F.H. Wittmann, T. Zhao, E.H. Lehmann, Neutron imaging of water penetration into cracked steel reinforced concrete, Physica B 405 (2010) 1866–1871, doi:10.1016/j.physb.2010.01.065.

[32] F.H. Kim, D. Penumadu, D.S. Hussey, Water distribution variation in partially saturated granular materials using neutron imaging, J. Geotech. Geoenviron. 138 (2012) 147–154.

[33] Y. Zhao, S. Gong, X. Hao, Y. Peng, Y. Jiang, Effect loading rate and bedding on the dynamic fracture toughness of coal: laboratory experiments, Eng. Fract. Mech. 178 (2017) 375–391.

[34] Y. Zhao, G. Zhu, C. Zhang, S. Liu, D. Elsworth, T. Zhang, Pore-scale reconstruction and simulation of non-Darcy flow synthetic porous rocks, J. Geophys. Res. Solid Earth 123 (2018) 2770–2786.

[35] N. Cueto, D. Benavente, J. Martínez-Martínez, M.A. García-del-cura, Rock fabric, pore geometry and mineralogy effects on water transport in fractured dolostones, Eng. Geol. 107 (2009) 1–15.

[36] A. Marmur, Capillary rise and hysteresis in periodic porous media, J. Colloid Interfaces Sci. 129 (1989) 278–285.

[37] Y. Zhao, Y. Wu, S. Han, S. Xue, G. Fan, Z. Chen, A.El Abd, Water sorptivity of unsaturated fractured sandstone: Fractal modeling and neutron radiography experiment, Adv. Water Resour. 130 (2019) 172–183.

[38] V. Cnudde, M. Dierick, J. Vlassenbroeck, B. Masschaele, E. Lehmann, E. Jacobs, L.V. Hoorebeke, High-speed neutron radiography for monitoring the water absorption by capillarity in porous materials, Nucl. Instrum. Meth. B 266 (2008) 155–163.

[39] R. Lucas, Rate of capillary ascension of liquids, Kolloid Z. 23 (1918) 15–22.

[40] E.W. Washburn, The dynamics of capillary flow, Phys. Rev. 17 (1921) 273–283.

[41] J.M. Bell, F.K. Cameron, The flow of liquids through capillary spaces, J. Phys. Chem. 10 (1906) 658–674.

[42] W.H. Green, G.A. Ampt, Studies on soil physics, J. Agric. Sci. 4 (1911) 1–24.

[43] H.E. Cude, G.A. Hulett, Some properties of charcoals, J. Am. Chem. Soc. 42 (1920) 391–401.

[44] E.K. Rideal, On the flow of liquids under capillary pressure, the London, Edinburgh, and Dublin philosophical magazine and, J. Sci. 44 (1922) 1152–1159.

[45] M.A. Bosanquet, On the flow of liquids under capillary pressure, the London, Edinburgh, and Dublin philosophical magazine and, J. Sci. 45 (1923) 525–531.

[46] H. Pleinert, H. Sadouki, F.H. Wittmann, Determination of moisture distributions in porous building materials by neutron transmission analysis, Mater. Struct. 31 (1998) 218–224, doi:10.1007/BF02480418.

[47] D.R.M. Brew, F.C. de Beer, M.J. Radebe, R. Nshimirimana, P.J. McGlinn, L.P. Aldridge, T.E. Payne, Water transport through cement-based barriers-A preliminary study using neutron radiography and tomography, Nucl. Instrum. Meth. A 605 (2009) 163–166, doi:10.1016/j.nima.2009.01.146.

[48] Y. Zhao, S. Xue, S. Han, Z. Chen, S. Liu, D. Elsworth, L. He, J. Cai, J. Liu, D. Chen, Effects of microstructure on water imbibition in sandstones using X-ray computed tomography and neutron radiography, J. Geophys. Res. Solid Earth 122 (2017) 4963–4981, doi:10.1002/2016JB013786.

[49] M.F. Middleton, K. Li, F.D. Beer, Spontaneous imbibition studies of Australian reservoir rocks with neutron radiography, in: Proceedings of the SPE Western Region Meeting, 30, Irvine, C.A., U.S.A., 2005, p. 93634, doi:10.2118/93634-MS.

[50] M. Kang, H.Z. Bilheux, S. Voisin, C.L. Cheng, E. Perfect, J. Horita, J.M. Warren, Water calibration measurements for neutron radiography : application to water content quantification in porous media $, Nucl. Instrum. Meth. A 708 (2013) 24–31, doi:10.1016/j.nima.2012.12.112.

[51] M. Kang, E. Perfect, C.L. Cheng, H.Z. Bilheux, J. Lee, J. Horita, J.M. Warren, Multiple pixel-scale soil water retention curves quantified by neutron radiography, Adv. Water Resour. 65 (2014) 1–8, doi:10.1016/j.advwatres.2013.12.004.

[52] R.D. Laughlin, J.E. Davies, Some aspects of capillary absorption in fibrous textile wicking, Text. Res. J. 31 (1961) 904–910.

[53] A.S. Balankin, &B.E. Elizarraraz, Hydrodynamics of fractal continuum flow, Phys. Rev. E 85 (2012) 025302, doi:10.1103/PhysRevE.85.025302.

[54] A.S. Balankin, R. Garci Paredes, O. Susarrey, D. Morales, F.C. Vacio, Kinetic roughening and pinning of two coupled interfaces in disordered media, Phys. Rev. Lett. 96 (2006) 056001, doi:10.1103/PhysRevLett.96.056101.

[55] A.S. Balankin, &O. Susarrey, Scaling properties of pinned interfaces in fractal media, Phys. Rev. Lett. 90 (2003) 7–10, doi:10.1103/PhysRevLett.90.096101.

[56] J. Cai, B. Yu, A discussion of the effect of tortuosity on the capillary imbibition in porous media, Transp. Porous Med. 89 (2011) 251–263, doi:10.1007/s11242-011-9767-0.

[57] P.G. Toledo, R.A. Novy, H.T. Davis, L.E. Scriven, Hydraulic conductivity of porous media at low water content, Soil Sci. Soc. Am. J. 54 (1990) 673–679.

[58] D.A. Lockington, &J. Parlange, Anomalous water absorption in porous materials, J. Phys. D Appl. Phys. 36 (2003) 760–767.

[59] D. Swartzendruber, Non-Darcy behavior and the flow of water in unsaturated soils, Soil Sci. Soc. Am. J. 27 (1963) 491–495.

[60] H. Sun, M.M. Meerschaert, Y. Zhang, Y. Zhu, Y. Chen, A fractal Richards' equation to capture the non-Boltzmann scaling of water transport in unsaturated media, Adv. Water Resour. 52 (2013) 292–295, doi:10.1016/j.advwatres.2012.11.005.

[61] D. Ben-Avraham, S. Havlin, Diffusion and Reactions in Fractals and Disordered Systems, Cambridge University Press, 2000, doi:10.1017/CBO9780511605826.
[62] M. Küntz, P. Lavallée, Experimental evidence and theoretical analysis of anomalous diffusion during water infiltration in porous building materials, J. Phys. D Appl. Phys. 34 (2001) 2547–2554, doi:10.1088/0022-3727/34/16/322.
[63] J. Bacri, M. Rosen, D. Salin, L. Ultrasms, U. Pierre, Capillary hyperdiffusion as a test of wettability, Europhys. Lett. E 11 (1990) 127–132, doi:10.1209/0295-5075/11/2/006.
[64] P. Lavall, K. Michel, Anomalous spreading of a density front from an infinite continuous source in a concentration-dependent lattice gas automaton diffusion model, J. Phys. D Appl. Phys. 36 (2003) 1135–1142.
[65] J.H. Cushman, D. O'Malley, M. Park, Anomalous diffusion as modeled by a nonstationary extension of Brownian motion, Phys. Rev. E 79 (2009) 1–4, doi:10.1103/PhysRevE.79.032101.
[66] Y. Pachepsky, D. Timlin, W. Rawls, Generalized Richards'equation to simulate water transport in unsaturated soils, J. Hydrol. 272 (2003) 3–13.
[67] E. Gerolymatou, I. Vardoulakis, R. Hilfer, Modelling infiltration by means of a nonlinear fractional diffusion model, J. Phys. D Appl. Phys. 39 (2006) 4104–4110, doi:10.1088/0022-3727/39/18/022.
[68] A.EI Abd, S.E. Kichanov, S.E. Nazarov, K.M. Kozlenko, K.M. Badawy, Determination of moisture distribution in porous building bricks by neutron radiography, Appl. Radiat. Isot. 156 (2020) 108970.
[69] R. Bruce, A. Klute, The measurement of soil moisture diffusivity, Soil Sci. Soc. Am. J. 20 (1958) 458–462.
[70] S. Chen, Estimating the hydraulic conductivity and diffusivity in unsaturated porous media by fractal capillary model, J. Chin. Inst. Eng. 21 (1998) 449–458, doi:10.1080/02533839.1998.9670407.
[71] D. Gimknez, E. Perfect, W.J. Rawls, &Y. Pachepsky, Fractal models for predicting soil hydraulic properties: a review, Eng. Geol. 48 (1997) 161–183.
[72] A.A. Greenenko, A.V. Chechkin, N.F. Shul'ga, Anomalous diffusion and Lévy flights in channeling, Phys. Lett. A 324 (2004) 82–85, doi:10.1016/j.physleta.2004.02.053.
[73] M.M. Meerschaert, &C. Tadjeran, Finite difference approximations for fractional advection-dispersion flow equations, J. Comput. Appl. Math. 172 (2004) 65–77, doi:10.1016/j.cam.2004.01.033.
[74] C. Chen, Time-space fabric underlying anomalous diffusion, Chaos Soliton Fract. 28 (2006) 923–925, doi:10.1016/j.chaos.2005.08.199.
[75] A. Espejo, J.V. Giráldez, K. Vanderlinden, E.V. Taguas, A. Pedrera, A method for estimating soil water diffusivity from moisture profiles and its application across an experimental catchment, J. Hydrol. 516 (2014) 161–168, doi:10.1016/j.jhydrol.2014.01.072.
[76] D. Lockington, Estimating the sorptivity for a wide range of diffusivity dependence on water content, Transp. Porous Med. 10 (1993) 95–101, doi:10.1007/BF00617513.
[77] M.B. Parlange, S.N. Prasad, J.Y. Parlange, M.J.M. Romkens, Extension of the Heaslet-Alksne technique to arbitrary soil water diffusivities, Water Resour. Res. 28 (1992) 2793–2797.
[78] G.S. Campbell, A simple method for determining unsaturated conductivity from moisture retention data, Soil Sci. 117 (1974) 311–314, doi:10.1097/00010694-197406000-00001.
[79] D. Lockingtonl, J. Parlange, J. Dux, Sorptivity and the estimation of water penetration into unsaturated concrete, Mater. Struct. 32 (1999) 342–347.
[80] J.J. Meyer, A.W. Warrick, Analytical expression for soil water diffusivity derived from horizontal infiltration experiments, Soil Sci. Soc. Am. J. 54 (1990) 1547–1552, doi:10.2136/sssaj1990.03615995005400060006x.
[81] C.L. Cheng, M. Kang, E. Perfect, S. Voisin, J. Horita, HZ. Bilheux, J.M. Warren, D.L. Jacobson, D.S. Hussey, Average soil water retention curves measured by neutron radiography, Soil Sci. Soc. Am. J. 76 (2011) 1184–1191, doi:10.2136/sssaj2011.0313.
[82] M.D. Abràmofff, P.J. Magalhães, S.J. Ram, Image processing with ImageJ Part II, Biophotonics Int. 11 (2005) 36–43, doi:10.1117/1.3589100.
[83] C.A. Schneider, W.S. Rasband, K.W. Eliceiri, NIH image to ImageJ: 25 years of image analysis, Nat. Methods 9 (2012) 671–675, doi:10.1038/nmeth.2089.
[84] I.S. Anderson, R.L. McGreevy, H.Z. Bilheux, Neutron Imaging and Applications, Springer, US, 2009, doi:10.1007/978-0-387-78693-3.
[85] R. Hassanein, E. Lehmann, P. Vontobel, Methods of scattering corrections for quantitative neutron radiography, Nucl. Instrum. Meth. A 542 (2005) 353–360, doi:10.1016/j.nima.2005.01.161.
[86] R. Hassanein, F. de Beer, N. Kardjilov, E. Lehmann, Scattering correction algorithm for neutron radiography and tomography tested at facilities with different beam characteristics, Physica B 385–386 (2006) 1194–1196, doi:10.1016/j.physb.2006.05.406.
[87] D.S. Hussey, D.L. Jacobson, M. Arif, K.J. Coakley, D.F. Vecchia, *In situ* fuel cell water metrology at the NIST neutron imaging facility, J. Fuel Cell Sci. Technol. 7 (2010) 021024, doi:10.1115/1.3007898.
[88] J. Cai, B. Yu, M. Mei, L. Luo, Capillary rise in a single tortuous capillary, Chin. Phys. Lett. 27 (2010) 1–4, doi:10.1088/0256-307X/27/5/054701.
[89] L. You, J. Cai, Y. Kang, A fractal approach To spontaneous imbibition height in natural porous media, Int. J. Mod. Phys. C 24 (2013) 1350063, doi:10.1142/S0129183113500630.
[90] B.V. Belleghem, R. Montoya, J. Dewanckele, N.V.D. Steen, I.D. Graeve, J. Deconinck, V. Cnudde, K.V. Tittelboom, N.D. Belie, Capillary water absorption in cracked and uncracked mortar-A comparison between experimental study and finite element analysis, Constr. Build. Mater. 110 (2016) 154–162.
[91] K. Li, H. Zhao, Fractal prediction model of spontaneous imbibition rate, Transp. Porous Med. 91 (2012) 363–376.
[92] J. Carmeliet, O.C.G. Adan, H. Hens, Determination of the liquid water diffusivity from transient moisture transfer experiments, J. Build. Phys. 27 (2004) 277–305, doi:10.1177/1097196304042324.
[93] L. Pel, Moisture transport in porous building materials, Sci. Technol. Eur. Cult. Herit. 41 (1991) 593–596.
[94] M.I. Nizovtsev, S.V. Stankus, A.N. Sterlyagov, V.I. Terekhov, V.I. Khairulin, Experimental determination of the diffusitives of moisture in porous materials in capillary and sorption moistening, J. Eng. Phys. Thermophys. 78 (2005) 68–74, doi:10.1007/s10891-005-0031-8.
[95] L. He, S. Han, H. Wang, L. Hao, M. Wu, G. Wei, Y. Wang, Y. Liu, K. Sun, D. Chen, Design of real-time neutron radiography at China advanced research reactor, Phys. Procedia 43 (2013) 48–53, doi:10.1016/j.phpro.2013.03.006.